Journal of Structural Geology, Vol. 12, No. 1, pp. 139 to 143, 1990
Printed in Great Britain

0191-8141/90 $03.00+0.00

Brevia

MICROCOMPUTER TECHNIQUES AND APPLICATIONS

Automated two-dimensional strain analysis from deformed elliptical markers using an image analysis system

KYUICHI KANAGAWA*

Department of Geology, University of Tokyo, Tokyo 113, Japan

(*Received* 18 *April* 1989; *accepted in revised form* 18 *August* 1989)

Abstract—An image analysis system is used to automate data collection from deformed elliptical markers and calculate strain using computer programs. In the image analysis, best-fit ellipses are calculated for individual binarized markers, and their axial ratios and long-axis orientations are used for strain calculations. The precision of data obtained by our system is within ±11% for axial ratios and within ±3° for long-axis orientations when a marker has an area larger than 360 pixels in an image area of 512 × 480 pixels, and is located in the central part of 256 × 240 pixels. An example of strain analysis from 275 ooids in a deformed oolitic limestone shows that the strain ellipse calculated from the data obtained by image analysis has a ~3% higher axial ratio and a 2.6° difference in long-axis orientation compared to manual methods. Finite strain analyses can be done automatically and precisely in a short time by using image analysis methods.

INTRODUCTION

THE shape and orientation of elliptical markers on plane sections of deformed rocks have been extensively used in finite strain analysis, and many techniques for estimating strains from such data have been proposed (e.g. Ramsay 1967, Dunnet 1969, Elliott 1970, Matthews *et al.* 1974, Shimamoto & Ikeda 1976, Lisle 1977a,b, Robin 1977). However, the analysis usually requires considerable time for data collection and strain calculation. Although several computer programs have been devised in order to calculate strains automatically (e.g. Dunnet & Siddans 1971, Matthews *et al.* 1974, Peach & Lisle 1979), the data needed for the analysis, such as axial lengths and orientations of markers, still need to be measured manually, a time-consuming task. Recently, digitization of graphic images using an image analysis system or a digitization tablet has been applied to the collection of such data (Simigian & Starkey 1986, Whalley 1987). These are useful methods for data collection, because they can be readily automated to provide a large quantity of data rapidly. This paper describes the use of an image analysis system for automating strain analysis of deformed elliptical markers. The method will be illustrated by an example of ooids in a deformed oolitic limestone.

* Present address: Department of Geology and Geography, University of Massachusetts, Amherst, MA 01003, U.S. A.

DATA COLLECTION WITH AN IMAGE ANALYSIS SYSTEM

The image analysis system used here is composed of an image processor with image memories of 512 × 480 pixels (NEXUS 6400 system), a 16-bit host microcomputer and a monochrome video camera (Fig. 1). The image processor is connected to the host computer via a GP-IB interface. An analogue image of graphic data obtained through the video camera is digitized by an A/D converter (Fig. 1) and stored in an image memory. A digitized image is represented by a 512 × 480 matrix **F** whose element f_{ij} gives the brightness at pixel (i, j). The digitized image is then binarized so that **F** is transformed into another matrix **G** whose element g_{ij} is expressed as follows:

$$g_{ij} = \begin{cases} 1 & (f_{ij} \leq t) \\ 0 & (f_{ij} > t) \end{cases}, \qquad (1)$$

where t is a threshold value of brightness. The binary image is stored in another image memory. The computer program recognizes individual markers by following the pixels with $g_{ij} = 1$, and calculates on each marker parameters such as the area, center of gravity, the length of perimeter, the maximum length and the width at a right angle to it, and the angle between the direction of maximum length and the horizontal line. These parameters are recorded in a data file on disk.

Because traced markers show an abrupt drop in brightness below background, a threshold value is easily

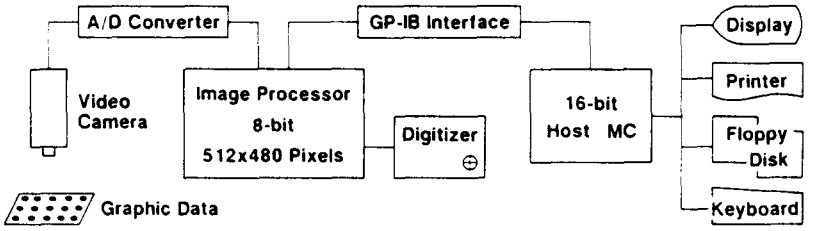

Fig. 1. An image analysis system. A/D converter: analogue-to-digital converter. GP–IB interface: interface using a general purpose interface bus. MC: microcomputer unit.

determined in the binarizing procedure and marker boundaries will be correctly recognized. Tracings of elliptical markers, rather than photographs, are therefore better as graphical data and were used in this study, although it is possible to use photographs of specimens when the marker boundaries are clearly distinguished.

A binarized marker is strictly a polygon composed of pixels (Fig. 2). In image analysis, its maximum length is defined as the maximum distance between two peripheral pixels, and the width as the distance between two tangent lines parallel to the direction of maximum length (Fig. 2a). The direction of maximum length does not necessarily coincide with the long axis of the marker. For example, a rectangle gives the maximum length in two diagonal directions. It therefore gives rise to significant errors not only in axial ratio but also in long-axis orientation to take the maximum length and the width as the axial lengths of a binarized marker. In order to avoid such errors, a best-fit ellipse is calculated on each marker using the least-squares method (cf. Simigian & Starkey 1986).

An ellipse centered at the origin of an x–y co-ordinate system can be written as an equation:

$$ax^2 + 2bxy + cy^2 = 1. \tag{2}$$

Let the center of gravity of a binarized marker be located at the origin, and the position of the ith peripheral pixel be (x_i, y_i), where $i = 1, 2, \ldots, N$. The sum of squared deviations from an ellipse is then:

$$S = \Sigma\,(ax_i^2 + 2bx_iy_i + cy_i^2 - 1)^2, \tag{3}$$

where the summation sign implies summing from 1 to N. Because S has to be minimized in order to obtain the best-fit ellipse, the partial differentials should equal zero:

$$\frac{\partial S}{\partial a} = \frac{\partial S}{\partial b} = \frac{\partial S}{\partial c} = 0 \tag{4}$$

which gives:

$$\begin{aligned} a\Sigma x_i^4 + 2b\Sigma x_i^3y_i + c\Sigma x_i^2y_i^2 &= \Sigma x_i^2 \\ a\Sigma x_i^3y_i + 2b\Sigma x_i^2y_i^2 + c\Sigma x_iy_i^3 &= \Sigma x_iy_i \\ a\Sigma x_i^2y_i^2 + 2b\Sigma x_iy_i^3 + c\Sigma y_i^4 &= \Sigma y_i^2. \end{aligned} \tag{5}$$

Using the solutions (a, b, c) of equations (5), the axial lengths and long-axis orientation of the best-fit ellipse are obtained by the following equations:

$$L = \frac{a + c \pm \sqrt{(a + c)^2 - 4(ac - b^2)}}{2} \tag{6}$$

$$\tan 2\phi = \frac{2b}{a - c}. \tag{7}$$

These axial lengths of the best-fit ellipse, and the angle between the long axis and the horizontal line (Fig. 2b) are recorded and used for strain calculations.

PRECISION OF DATA OBTAINED BY IMAGE ANALYSIS

Errors in image analysis are introduced by the following factors: (1) approximation of image by pixels (digitizing); (2) distortion of image caused by lens aberration of the video camera; and (3) uneven brightness of image caused by lighting and shading which is a phenomenon of decrease in brightness toward the periphery of image. Uneven brightness significantly affects marker boundary positions during the binarizing procedure. The effect of digitizing varies depending on area and axial ratio of a marker, whereas the effects of lens aberration, lighting and shading vary depending on marker locations. The errors introduced by these factors do not vanish, although they can be reduced by using an image processor with higher resolution, by using a lens with less

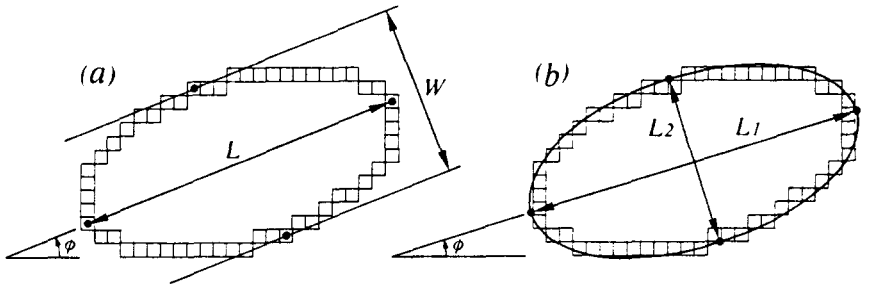

Fig. 2. Definition of the long and short axes of a binarized elliptical marker. (a) The maximum length (L), the width (W) and the direction of maximum length (ϕ). (b) The long and short axes (L_1 and L_2), and the long-axis orientation (ϕ) of the best-fit ellipse.

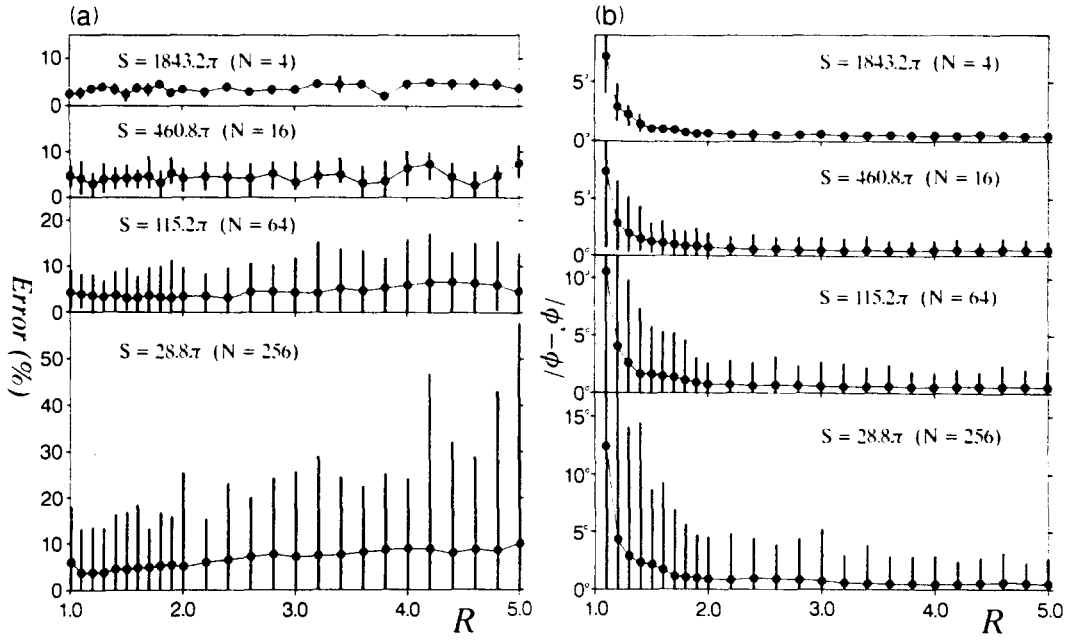

Fig. 3. Errors in axial ratio (a) and in long-axis orientation (b) of binarized ellipses with four different areas (S) and variable axial ratios (R). Every ellipse has the same orientation with $\varphi = 0°$. Closed circle and bar represent the average and range of errors, respectively, for ellipses with each axial ratio.

aberration, and by lighting more uniformly and correcting for shading.

The precision of data obtained under our present system is investigated here by using computer-drawn ellipses with different areas and axial ratios. The areas of these ellipses in an image area of 512 × 480 pixels are 1843.2π, 460.8π, 115.2π and 28.8π pixels, and the numbers of ellipses in the image are 4, 16, 64 and 256, respectively. Axial ratios of these ellipses range from 1.0 to 5.0. Let R and ϕ be the axial ratio and long-axis orientation of a computer-drawn marker ellipse ($\phi = 0°$ here), and let R' and ϕ' be the axial ratio and long-axis orientation of the best-fit ellipse of the binarized marker. Percentage error in axial ratio is calculated from the following equation.

$$\text{error } (\%) = (|R' - R|/R) \times 100. \quad (8)$$

The error in long-axis orientations is represented by the difference between ϕ and ϕ'; $|\phi' - \phi|$. The results are shown in Fig. 3 and summarized in Table 1. The error in axial ratio clearly increases with decreasing marker areas, whereas it slightly increases with increasing axial ratios for ellipses having the same area (Fig. 3a). The error in long-axis orientation slightly increases with decreasing marker area, whereas it exponentially decreases with increasing axial ratio (Fig. 3b).

The variation in errors depending on marker location in an image has been investigated for ellipses having an area of 115.2π. An image is divided into four equivalent domains each of which contains 16 ellipses: (1) central part; (2) top and bottom sides; (3) right and left sides; and (4) corners. Errors in axial ratio and long-axis orientation in each domain are separately determined (Fig. 4 and Table 1). The data obtained are most precise in domain (1) and least precise in domain (4).

These results indicate that, under the present system, markers larger than 115.2π (about 360) pixels in the central 256 × 240 pixels of an image give errors less than 11% in axial ratio and less than 3° in long-axis orientation (Table 1).

STRAIN CALCULATIONS

Once axial lengths and orientations of a suite of markers have been obtained by image analysis, strains can be automatically calculated using computer programs. The programs used in this study incorporate five different strain calculation methods: (1) the slope method (Ramsay 1967); (2) the method of means (Lisle 1977a); (3) the method of Shimamoto & Ikeda (1976); (4) the R_f/ϕ method (Dunnet 1969); and (5) the θ-curve method (Lisle 1977b) which is a modified R_f/ϕ method. The former two methods provide only an imprecise

Table 1. Summary of error data shown in Figs. 3 and 4. The percentage errors in axial ratio are shown by the ranges of average and maximum errors, while the errors in long-axis orientation are represented by three axial ratios for above which the maximum error becomes less than 3°, 2° and 1°

S	Domain	Error (%)		$\lvert\phi'-\phi\rvert$		
		average	maximum	<3°	<2°	<1°
1843.2π	all	1.80-5.05	2.27-6.00	1.4	1.5	2.6
460.8π	all	2.50-7.62	5.43-11.40	1.5	2.2	—
115.2π	(1)	1.56-6.68	3.23-11.48	1.2	1.5	1.7
	(2)	1.25-6.91	3.10-12.72	1.6	1.8	2.8
	(3)	3.68-8.37	6.80-17.31	1.6	1.8	2.8
	(4)	2.77-8.13	5.78-15.68	2.0	3.8	—
	all	3.06-6.70	6.80-17.31	2.0	3.8	—
28.8π	all	3.48-10.43	13.28-57.55	3.6	—	—

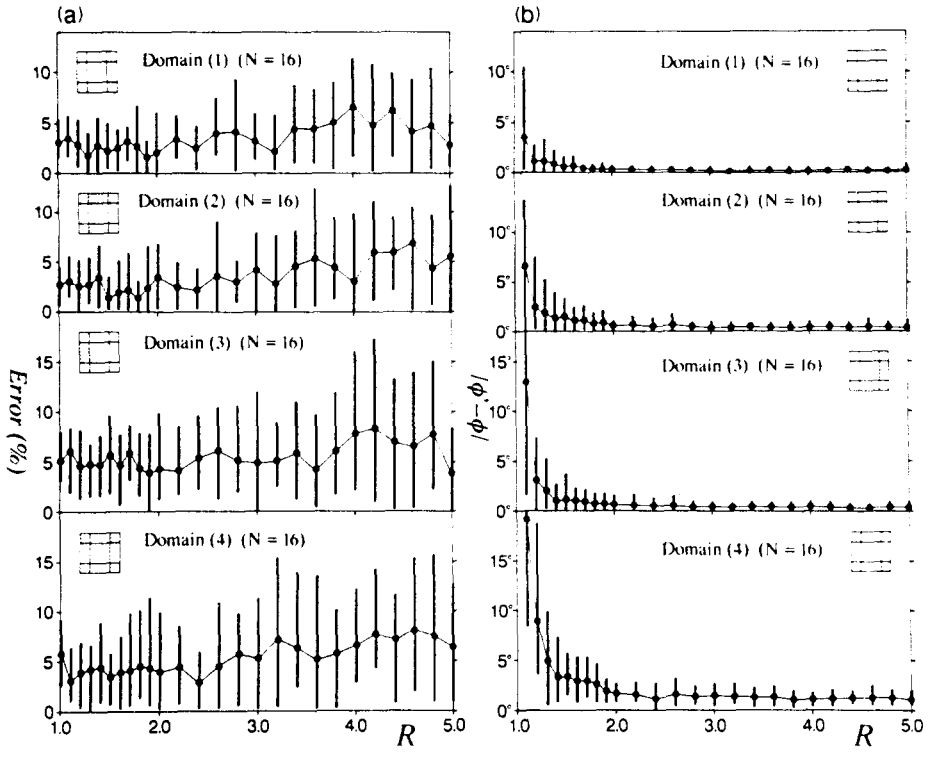

Fig. 4. Errors in axial ratio (a) and in long-axis orientation (b) of binarized ellipses with variable axial ratios (R) in four different domains (dotted). Every ellipse has the same orientation with $\phi = 0°$ and the constant area of 115.2π pixels. Closed circles and bars are the same as those in Fig. 3.

estimate of the axial ratio of the strain ellipse (R_s), whereas the latter three methods provide a better estimate of the shape and orientation of the strain ellipse. Description of these methods is avoided here, because the reader can refer not only to the above references for full descriptions, but also to Hanna & Fry (1979), Paterson (1983), Ramsay & Huber (1983), Lisle (1985) and Babaie (1986) for brief descriptions.

The computer programs for calculating strains were written in BASIC and are available from the author. The programs using the R_f/ϕ technique were written based on the procedures described by Lisle (1985) referring to the program STRANE of Dunnet & Siddans (1971) and the program THETA of Peach & Lisle (1979). For a set of R_f/ϕ data, the symmetry test or the θ-distribution test is applied. The symmetry check is also possible from a ϕ frequency diagram or a contour map of the R_f/ϕ data (cf. Ramsay & Huber 1983, p. 83). If the data satisfy symmetry conditions, an optimum value of strain ratio is automatically determined using the R_f/ϕ method or the θ-curve method. If they fail, the data distribution is regarded as asymmetric and the unstraining subroutine which is part of STRANE is called. This procedure successively imposed an incremental reciprocal strain until the symmetry of the θ-distribution is maximized, and gives a possible solution for the axial ratio and orientation of the strain ellipse.

EXAMPLE

As an example, data were collected from the photomicrograph of an Ordovician oolitic limestone of North Wales, which is shown in fig. 5.7 of Ramsay & Huber (1983, p. 79). Then 275 ooids were traced from an enlarged photocopy of the photomicrograph. Their axial ratios and long-axis orientations were first measured using a caliper and a protractor, and next obtained using the image analysis system. In the image analysis, the traced ooids were divided into four groups so that all digitized ooids occupy an area larger than 360 pixels, and the central parts of the four different images were used for data collection. The calculated strain ratios and long-axis orientations of the strain ellipse obtained in these two ways are listed in Table 2 together with those given in Ramsay & Huber (1983).

The three means of the data obtained manually agree very well with those of Ramsay & Huber (1983). The means of the data obtained by image analysis correlate reasonably well with, but are systematically higher than, those obtained manually and by Ramsay & Huber (1983).

The method of Shimamoto & Ikeda (1976) and the θ-curve method give the most conservative and consistent R_s values. The R_f/ϕ method gives slightly higher values than the above two methods. In contrast, the R_s value estimated using the R_f/ϕ method by Ramsay & Huber (1983) is much higher than those in this study, and even higher than the three means given by them. Because the means always overestimate R_s unless markers are initially circular (Lisle 1977a), this higher value must be incorrect due to the visual fitting of standard R_f/ϕ curves to data. The R_s values calculated from the data obtained by the image analysis using the method of Shimamoto & Ikeda (1976), the θ-curve method and the R_f/ϕ method again take higher values than the corresponding values from the data obtained manually.

Table 2. Calculated strain ratios (R_s) and long-axis orientations of the strain ellipse from the data obtained manually and by image analysis compared with those given by Ramsay & Huber (1983)

Method	Ramsay & Huber (1983) (N=280)	This study (N=275)			
		Data obtained manually		Data obtained by image analysis	
Slope (long/short)	—	1.59		1.63	
Arithmetic mean $\overline{Rf}$	1.67	1.68		1.74	
Geometric mean G	1.64	1.64		1.69	
Harmonic mean H	1.60	1.61		1.66	
Shimamoto & Ikeda (1976)	—	1.52	51.9°	1.57	54.5°
Rf/ϕ (Dunnet & Siddans 1971)	1.7*	1.56	52.6°	1.59	55.2°
θ-curve (Peach & Lisle 1979)	—	1.52		1.56	

*Obtained by visual fitting standard curves to data.

The calculated long-axis orientation of the strain ellipse by the R_f/ϕ and θ-curve methods agrees well with that derived from the method of Shimamoto & Ikeda (1976) (Table 2). It should be noted that the long-axis orientations calculated from the data obtained manually (52.6° and 51.9°) are exactly perpendicular to the direction of extension fissures (−38°) present in the photomicrograph of Ramsay & Huber (1983). When obtained by image analysis both these angles are greater by 2.6° (Table 2).

CONCLUSIONS

The above example shows that the strain ellipse calculated from the data obtained by image analysis has a ~3% higher axial ratio and a 2.6° difference in long-axis orientation compared to that from the manually measured data (Table 2). These values provide rough estimates of errors in data collection using our image analysis system from a suite of elliptical markers with variable axial ratios and orientations.

The greatest advantage of the use of an image analysis system in strain analysis is the speed with which it provides a quantity of data. The manual measurement of 275 ooids requires almost an entire day, whereas it takes less than 30 min for the data collection using the image analysis system. The time for strain calculation varies depending on quantity of data and methods used. For 275 ooids, it took less than 10 s for the calculation using the slope method, the method of means and the method of Shimamoto & Ikeda (1976), about 6 min for the R_f/ϕ method, and about 25 min for the θ-curve method. Because the method of Shimamoto & Ikeda (1976) provides results as precise as those of the θ-curve method, it is most efficient to use this method for the data which satisfied the symmetry check of the R_f/ϕ method. Strain analysis which has required considerable time and great effort hitherto can thus be done automatically and precisely in a very short time by using the image analysis system described here.

Acknowledgements—I thank Drs R. J. Lisle, S. Yoshida, E. A. Erslev, S. H. Treagus and an anonymous referee for helpful reviews of the manuscript. This study was supported by grants 61420015 and 62740455 from the Ministry of Education, Science and Culture of Japan, which is gratefully acknowledged.

REFERENCES

Babaie, H. A. 1986. A comparison of two-dimensional strain analysis methods using elliptical grains. *J. Struct. Geol.* **8**, 585–587.

Dunnet, D. 1969. A technique of finite strain analysis using elliptical particles. *Tectonophysics*, **7**, 117–136.

Dunnet, D. & Siddans, A. W. B. 1971. Non-random sedimentary fabrics and their modifications by strain. *Tectonophysics* **12**, 307–325.

Elliott, D. 1970. Determination of finite strain and initial shape from deformed elliptical objects. *Bull. geol. Soc. Am.* **81**, 2221–2236.

Hanna, S. S. & Fry, N. 1979. A comparison of methods of strain determination in rocks from southwest Dyfed (Pembrokeshire) and adjacent areas. *J. Struct. Geol.* **1**, 155–162.

Lisle, R. J. 1977a. Estimation of the tectonic strain ratio from the mean shape of deformed elliptical markers. *Geologie Mijnb.* **56**, 140–144.

Lisle, R. J. 1977b. Clastic grain shape and orientation in relation to cleavage from the Aberystwyth Grits, Wales. *Tectonophysics* **39**, 381–396.

Lisle, R. J. 1985. *Geological Strain Analysis: A Manual for the* R_f/ϕ *Technique*. Pergamon Press, Oxford.

Matthews, P. E., Bond, R. A. B. & Van Den Berg, J. J. 1974. An algebraic method of strain analysis using elliptical markers. *Tectonophysics* **24**, 31–67.

Paterson, S. R. 1983. A comparison of methods used in measuring finite strain from ellipsoidal objects. *J. Struct. Geol.* **5**, 611–618.

Peach, C. J. & Lisle, R. J. 1979. A FORTRAN IV program for the analysis of tectonic strain using deformed elliptical markers. *Computers Geosci.* **5**, 325–334.

Ramsay, J. G. 1967. *Folding and Fracturing of Rocks*. McGraw-Hill, New York.

Ramsay, J. G. & Huber, M. I. 1983. *The Techniques of Modern Structural Geology. Volume 1: Strain Analysis*. Academic Press, London.

Robin, P.-Y. F. 1977. Determination of geologic strain using randomly oriented strain markers. *Tectonophysics* **42**, T7–T16.

Shimamoto, T. & Ikeda, Y. 1976. A simple algebraic method for strain estimation from deformed ellipsoidal objects. 1. Basic theory. *Tectonophysics* **36**, 315–337.

Simigian, S. & Starkey, J. 1986. Automated grain shape analysis. *J. Struct. Geol.* **8**, 589–592.

Whalley, J. S. 1987. The use of a digitizing tablet to automate R_f/ϕ calculations. *J. Struct. Geol.* **9**, 501–502.